

Article

Zinc Presence during Mineral Formation Affects the Sorptive Reactivity of Manganese Oxide

Shiliang Zhao, Chenning Li, Pan Liu, Rixiang Huang, Emily M. Saad and Yuanzhi Tang *

School of Earth and Atmospheric Sciences, Georgia Institute of Technology, Atlanta, GA 30332-0340, USA; shiliang.zhao@eas.gatech.edu (S.Z.); m18801066306_1@163.com (C.L.); pan.liu@eas.gatech.edu (P.L.); rixiang.huang@eas.gatech.edu (R.H.); emily.saad@eas.gatech.edu (E.M.S.)

* Correspondence: yuanzhi.tang@eas.gatech.edu; Tel.: +1-404-894-3814

Received: 28 February 2018; Accepted: 27 March 2018; Published: 2 April 2018



Abstract: The sorptive reactivity of layered manganese (Mn) oxides is controlled by their layer and interlayer structure, which can be affected by processes such as metal coprecipitation. This study investigated the effects of Zn coprecipitation on the sorptive reactivity of δ -MnO₂, a common layered Mn oxide mineral. Selected cation (i.e., Cd) and anion (i.e., phosphate and arsenate) species were used to probe the changes in δ -MnO₂ sorptive reactivity. Cd uptake by δ -MnO₂ was suppressed by Zn coprecipitation but total metal uptake (Cd and Zn) was enhanced, indicating more available vacancy sites (e.g., smaller particle size and higher vacancy site density) in Zn-coprecipitated δ -MnO₂. Phosphate and arsenate sorption on δ -MnO₂ was significantly enhanced by Zn-coprecipitation, and the enhancement was more effective compared to Zn sorption on pure δ -MnO₂. X-ray diffraction and X-ray adsorption spectroscopy analysis did not detect the formation of surface precipitations and/or ternary complexes. The enhanced anion sorption on Zn-coprecipitated δ -MnO₂ was likely due to the compensation of negative surface charge by sorbed Zn, as well as the structural modifications introduced by Zn coprecipitation. Results from this study can provide a better understanding on the interactions between metal-coprecipitated Mn oxides and other species in natural environments.

Keywords: manganese oxides; zinc; coprecipitation; sorption; cadmium; arsenate; phosphate

1. Introduction

Manganese oxides (MnO_x), especially layered phyllosulfates, are important metal oxides in terrestrial and oceanic environments [1–3]. Because of the high surface area, negative surface charge, vacancy sites, and high oxidative potential, phyllosulfates have a strong tendency to interact with and strongly influence the fate and transport of trace metals, such as Ni [4–8], Co [6,8–13], Pb [7,14–18], Cu [6,19,20], Zn [4,7,17,21–23], and Cd [24,25]. Phyllosulfates can interact with metals in different ways (e.g., sorption, coprecipitation, incorporation), which in turn can affect the property and reactivity of the host mineral phases. During sorption onto δ -MnO₂, metal cations can either directly incorporate into vacancy sites, or form surface sorption complexes above or below vacancies sites and/or at edge sites [2,26]. The ratio between incorporation and surface complexation (referred to as compatibility) is metal specific, and was suggested to be dependent on the differences in atomic size and charge between foreign metal cations and Mn(III, IV) [2,11], as well as the metal cation crystal field stability energy (CFSE) [27]. Sorption of metal cations on pre-formed MnO_x (i.e., sorption) can replace interlayer Mn(II) and alkaline cations [28,29], and compensate for the negative surface charge, thus affecting the reactivity of MnO_x towards other species [29–31]. In comparison, the presence of metal cations during MnO_x mineral formation (i.e., coprecipitation) can cause more significant changes in MnO_x structure, such as layer stacking, average oxidation state [7,11,13,32], vacancy site density, and layer symmetry [10], which also lead to modified mineral reactivity. For example, the presence of Ni, Co,

Fe, and Cu during birnessite formation was found to significantly modify birnessite thermal stability, sorptive reactivity towards Pb, and oxidative reactivity towards As(III) [7,11,13,32].

The effects of metal coprecipitation on layered Mn oxides are also metal-specific. The compatibility of foreign metal ions in birnessite layers is $\text{Fe}^{3+} < \text{Ni}^{2+} < \text{Co}^{3+}$ and the interruption of birnessite structures is in the reverse order $\text{Fe}^{3+} > \text{Ni}^{2+} > \text{Co}^{3+}$ [7,11,13]. Zn is an essential element and its biogeochemical cycles are affected by organic matters and Fe/Mn oxide minerals in soils and marine sediments [4,7,17,21–23,33]. Zn shows the least compatibility with Mn oxides compared to other transition metals such as Ni or Co. As a result, upon sorption onto MnO_x , Zn^{2+} never incorporates into vacancy sites, but always exists as sorbed species above/below vacancy sites [27] and sometimes edge sites [34]. The local coordination environment of surface-sorbed Zn^{2+} is preferably tetrahedral ($^{\text{IV}}\text{Zn}$) at low Zn loadings and octahedral ($^{\text{VI}}\text{Zn}$) at high Zn loadings [2,35,36], although it is also dependent on the crystallinity of the host MnO_x phase [21]. A recent study by Grangeon et al. [21] found that Zn^{2+} sorption on $\delta\text{-MnO}_2$ caused crystal dissolution, decrease of coherent scattering domain size, decrease of layer Mn(III) content, and increase of vacancy site density. Similar effects have not been observed for the sorption of other metal cations on MnO_x . When Zn^{2+} was added during the formation of biogenic MnO_x , it was found to interrupt the mineral layer stacking [36]. Our recent study showed that the presence of Zn^{2+} during abiotic $\delta\text{-MnO}_2$ formation has more significant impacts on $\delta\text{-MnO}_2$ structure compared to Zn sorption on pure $\delta\text{-MnO}_2$ [37]. These studies demonstrate the significant effects of Zn^{2+} treatment (either sorption or coprecipitation) on $\delta\text{-MnO}_2$ structure, which can potentially affect the sorptive reactivity of $\delta\text{-MnO}_2$. However, systematic investigations are still missing on the effects of Zn-coprecipitation on MnO_x reactivities, such as those related to sorption or redox reactions.

This study systematically investigated the impact of Zn coprecipitation on the sorptive reactivity of $\delta\text{-MnO}_2$ toward both cations and anions. The Zn/Mn molar ratio used in this study was 0–0.2, which is within the range observed in the natural environment (0–0.005 in marine nodules and basin soils [38–40], as high as 0.03 in coal mine drainage treatment system [41] and 0.46 in contaminated sediments [42]). We used Cd^{2+} as a representative cation probe and phosphate and arsenate as representative anion probes to assess the change in $\delta\text{-MnO}_2$ sorptive reactivity. Cd is a toxic trace metal and its fate in the environment is strongly influenced by sorption onto metal oxyhydroxides, especially MnO_x [24,43,44]. Both phosphate and arsenate are important environmental anions, and their fate and transport are strongly influenced by interactions with geomedia [7,45–51]. Cd, phosphate, and arsenate sorption kinetics, isotherms, and pH edges on Zn-coprecipitated $\delta\text{-MnO}_2$ were compared with those on Zn-sorbed pure $\delta\text{-MnO}_2$ (hereafter referred to as Zn-sorbed $\delta\text{-MnO}_2$).

2. Methods

2.1. Synthesis of Pure and Zn-Coprecipitated $\delta\text{-MnO}_2$

All reagents used in this study were ACS (American Chemical Society) grade or higher. $\delta\text{-MnO}_2$ was synthesized [52] in the presence of varied concentrations of Zn^{2+} . A calculated amount of ZnSO_4 was dissolved in 160 mL of $0.2964 \text{ mol L}^{-1}$ MnSO_4 solution to achieve the desired Zn/ Mn_{total} ratio. This solution was pumped at a rate of 25 mL min^{-1} with a syringe pump into a beaker containing 160 mL of KMnO_4 (5.0 g) and 180 mL of NaOH (3.5 g) under vigorous stirring. The molar ratio of Zn/ Mn_{total} was 0, 0.01, 0.05, and 0.20. After overnight settlement, the solids were separated by vacuum filtration ($0.22 \mu\text{m}$), rinsed and dialyzed with deionized (DI) water, and freeze dried. Samples were labeled as pure, coppt0.01, coppt0.05, and coppt0.20 $\delta\text{-MnO}_2$ for the samples synthesized with initial Zn/Mn molar ratios of 0, 0.01, 0.05, and 0.20, respectively. A portion of the freezer-dried powders were digested using hydroxylamine hydrochloride and measured for elemental compositions (Zn, Mn) using inductively coupled plasma-mass spectrometry (ICP-MS) (Agilent 7500a) (Table 1).

Table 1. Initial Zn/Mn_{total} molar ratio in the synthesis suspension and final Zn/Mn molar ratio in the solid products.

Sample	Sample Label	Initial Zn/Mn Molar Ratio	Zn/Mn Molar Ratio in Final Solids	Zn Uptake (mmol/g)
Pure δ -MnO ₂	pure	0	0	0
Zn-coprecipitated δ -MnO ₂	coppt0.05	0.05	0.04	0.36
	coppt0.20	0.20	0.21	1.50
Zn-sorbed δ -MnO ₂	sorb0.07	0.07	0.06	0.42
	sorb0.20	0.20	0.15	0.99
	sorb0.30	0.30	0.19	1.30
	sorb0.60	0.60	0.31	1.69

2.2. Cation and Anion Sorption on Pure and Zn-Coprecipitated δ -MnO₂

CdCl₂, ZnSO₄, Na₂HPO₄, and Na₂HAsO₄ were used to make 1 mol L⁻¹ Cd²⁺, 1 mol L⁻¹ Zn²⁺, 2.5 mmol L⁻¹ phosphate, and 2.5 mmol L⁻¹ arsenate stock solutions, respectively. A total of 10 mg pure or Zn-coprecipitated δ -MnO₂ was suspended in 20 mL DI water and sonicated for 1 min to disperse the particles. For each sorption experiment, the calculated amount of stock solutions were added to achieve the desired sorbate concentration. The sorption isotherm and kinetic experiments were conducted at pH 6. The pH edge experiments were conducted at pH 4–8. The reaction vials were agitated end-to-end on an orbital shaker at 150 rpm. At certain time points, aliquots of the reaction suspension were taken and syringe filtered (0.22 μ m). Phosphate [53] and arsenate [54] concentrations in the filtrates were measured using colorimetric methods on a UV-vis spectrometer (Cary 60, Agilent). Zn and Cd concentrations were determined using ICP-MS.

For Cd²⁺ sorption, the ionic strength was at 0.1 mol L⁻¹ NaCl. Due to the relatively large pH fluctuation during sorption, 20 mmol L⁻¹ MES (2-(N-morpholino)ethanesulfonic acid) buffer was used to maintain the pH at 6. For phosphate and arsenate sorption, the ionic strength was at 10 mmol L⁻¹ NaCl. No buffers were used as the pH fluctuation throughout experiments was relatively small. At 0, 3, 12, and 22 h, HCl and NaOH solutions were used to adjust the small pH changes.

To examine the possible surface precipitation or ternary complexation between anions and pre-loaded Zn, X-ray diffraction (XRD) and X-ray sorption spectroscopy (XAS) analysis were conducted on the reaction products (details in Supporting Information, SI, Text S1). Both Langmuir and Freundlich models were used to fit the isotherm data. For kinetic data, pseudo first order, pseudo second order, and particle diffusion models were used to fit the data.

For Cd²⁺ sorption on Zn-coprecipitated δ -MnO₂, in order to investigate the overall metal cation uptake capacity, total metal uptake (both Cd²⁺ and Zn²⁺) was calculated using the following equation:

$$\text{Total metal uptake} = \text{initially loaded Zn} + \text{adsorbed Cd} - \text{desorbed Zn} \quad (1)$$

2.3. Cation and Anion Sorption on Zn-Sorbed δ -MnO₂

Based on previous studies and our recent study [37], when Zn is added during δ -MnO₂ formation, it exists as surface sorbed species, but can introduce significant structural modification. In order to compare the effects of Zn-coprecipitation-induced structural modification on δ -MnO₂ sorptive reactivity, we also conducted parallel experiments where pure δ -MnO₂ with Zn sorption (i.e., Zn-sorbed δ -MnO₂, with Zn concentrations comparable to the coprecipitation system) were used as the sorbent, with the subsequent addition of Cd²⁺, phosphate, and arsenate as sorbate.

Zn-sorbed δ -MnO₂ samples were produced by reacting 0.5 g L⁻¹ pure δ -MnO₂ with varied concentrations of ZnSO₄ (0.25–2 mmol L⁻¹) at pH 6 and 0.1 mol L⁻¹ NaCl background electrolyte. After shaking at 150 rpm for 24 h, the reaction reached steady state and the suspension was centrifuged at 13,000 rpm. The Zn concentration in the supernatant was measured by ICP-MS. Zn uptake was calculated by the difference of Zn concentration in the initial suspension and supernatant. After

centrifugation, the remaining wet paste (Zn-sorbed δ -MnO₂) was briefly rinsed with DI water, and resuspended in a small amount of DI water. Cd²⁺, phosphate, arsenate, and NaCl were added to the suspension following the procedures in Section 2.2 for sorption experiments. Sample labels are shown in Table 1.

3. Results and Discussion

3.1. Cation Sorption on Pure and Zn Coprecipitated δ -MnO₂

Cd sorption isotherms on Zn-coprecipitated δ -MnO₂ are shown in Figure 1A. Increasing initial Cd concentration resulted in a gradual increase in Cd uptake. The Langmuir model was used to fit the data (Figure 1A, Table 2). The maximum Cd uptake (C_{\max} , mmol g⁻¹) decreased slightly from 1.49 (pure δ -MnO₂) to 1.38 (coppt0.05) and 1.20 (coppt0.20), indicating the competitive sorption between Cd and pre-loaded Zn. This decrease was not significant, considering that the fitting errors of C_{\max} were in the range of 0.03–0.07. In order to compare Zn-coprecipitated and Zn-sorbed δ -MnO₂, sample sorb0.20 was also prepared by mixing 0.5 g L⁻¹ pure δ -MnO₂ and the calculated amount of ZnSO₄ (Zn/Mn = 0.2). The Zn loading on sample sorb0.20 ($Q = 0.99$ mmol g⁻¹) was much lower than the Zn coverage of the coppt0.20 sample ($Q = 1.5$ mmol g⁻¹), although they had the same initial Zn/Mn concentration. A similar phenomenon was also observed for biogenic MnO_x, i.e., Zn uptake by fungal MnO_x was higher when Zn was present during MnO_x formation, compared to Zn uptake by pre-formed pure MnO_x [36]. With less surface-loaded Zn, Cd sorption on sample sorb0.20 was, however, more suppressed (1.1 mmol g⁻¹) compared to sample coppt0.20 (1.2 mmol g⁻¹). This was likely caused by the structural modifications of δ -MnO₂ by Zn coprecipitation.

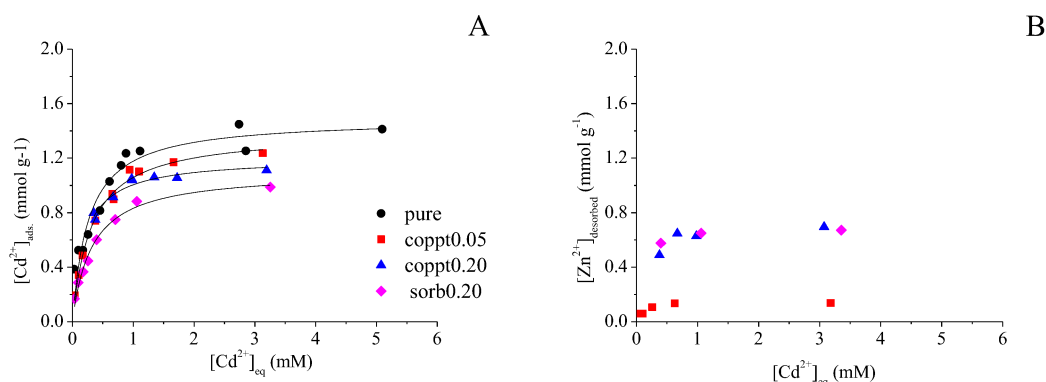


Figure 1. (A) Cd²⁺ sorption isotherms on pure, Zn-coprecipitated (coppt0.05, coppt0.20) and Zn-sorbed (sorb0.20) δ -MnO₂ samples. (B) Amount of Zn²⁺ release (desorption) during Cd²⁺ sorption. Solid lines are Langmuir model fitting results.

Table 2. Langmuir model fitting results of Cd²⁺, phosphate, and arsenate sorption isotherms on pure, Zn-coprecipitated, and Zn-sorbed δ -MnO₂.

Mn Oxide	Cd Isotherm			P Isotherm			As Isotherm		
	C_{\max}	K	R ²	C_{\max}	K	R ²	C_{\max}	K	R ²
pure	1.49	3.77	0.91	81.3	0.02	0.95	109.4	0.05	0.94
coppt0.05	1.38	3.19	0.99	120.4	0.04	0.96	162.2	0.07	0.99
coppt0.20	1.20	4.11	0.93	186.2	0.25	0.98	218.0	0.14	0.98
sorb0.20	1.10	3.08	0.99	-	-	-	-	-	-

Figure 1B shows the concentration of solution Zn during Cd sorption on samples coppt0.05, coppt0.20, and sorb0.20 δ -MnO₂. With increasing initial Cd concentrations, more Zn was released into the solutions. However, the concentration of sorbed Cd was always higher than released Zn.

This suggests that a fraction of Cd was sorbed via the exchange with Zn, and the rest of the Cd was sorbed on unoccupied surface sites. Because the surface sites of both coppt0.20 and sorb0.20 samples were already occupied by a large amount of Zn, they showed a similar amount of desorbed Zn (maximum $\sim 0.70 \text{ mmol g}^{-1}$), both higher than that of coppt0.05 (maximum $\sim 0.17 \text{ mmol g}^{-1}$). Total metal uptake (Equation (1)) was also calculated to compare the sorption capacity of different minerals (Figure 2). At low Cd concentrations, the total metal uptake increased with the increasing Cd concentration. The total metal uptake reached a plateau after $\sim 1 \text{ mmol L}^{-1} [\text{Cd}]_{\text{eq}}$ (i.e., equilibrium Cd concentration in the reaction suspension), suggesting the saturation of available surface sites for cation sorption. Although Zn coprecipitation with $\delta\text{-MnO}_2$ decreased Cd sorption (due to the pre-occupation of surface sites by Zn), the overall metal uptake by coppt0.20 sample ($\sim 1.9 \text{ mmol g}^{-1}$) was much higher than pure $\delta\text{-MnO}_2$ ($\sim 1.4 \text{ mmol g}^{-1}$), suggesting significant structural modifications by Zn coprecipitation, e.g., increased availability of surface sites for cation sorption.

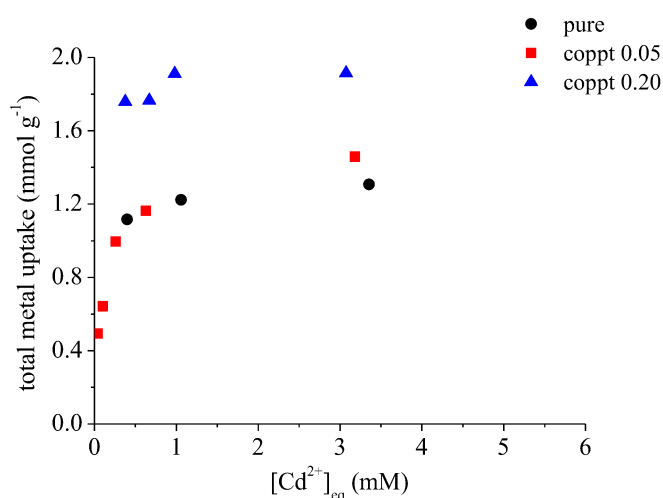


Figure 2. Total metal uptake (calculated by Equation (1)) on pure and Zn-coprecipitated $\delta\text{-MnO}_2$ samples.

3.2. Anion Sorption on Pure and Zn Coprecipitated $\delta\text{-MnO}_2$

3.2.1. Phosphate and Arsenate Sorption on Pure $\delta\text{-MnO}_2$

The phosphate and arsenate sorption kinetics (both with $100 \mu\text{mol L}^{-1}$ initial concentration) are shown in Figure 3A,B. Both pseudo first and second order kinetic models were used to fit the kinetic data (Figure S4), and the first order model yielded a better fit (Table 2 and Table S2). Arsenate sorption had a faster sorption rate constant (k) and reached a higher uptake capacity at equilibrium. Phosphate pH edge experiments (Figure 4) showed a gradual increase in phosphate uptake by pure $\delta\text{-MnO}_2$ with decreasing pH, reaching a maximum at $\text{pH} < 5$, consistent with previous studies [45,55,56].

Both phosphate and arsenate sorption reactions were fast and completed within a few hours (Figure 3). Therefore, a 24-h reaction time was chosen for phosphate and arsenate isotherm experiments, and the results are shown in Figure 3C,D. Both Langmuir and Freundlich models were used to fit the data (Figure S3) and the Langmuir model showed a better fit (Table 3 and Table S1). The maximum sorption capacity for phosphate and arsenate were 81.33 and $109.45 \mu\text{mol g}^{-1}$, respectively. Both are a magnitude lower than those of cations, consistent with previous studies [28,31,56–58]. The zero point charge (ZPC) of $\delta\text{-MnO}_2$ is around 2.8 [59], resulting in a negatively-charged surface under a wide range of pH. At the studied pH range, phosphate exists mainly as H_2PO_4^- and HPO_4^{2-} ($\text{pK}_a = 7.21$), while arsenate exists mainly as H_2AsO_4^- and HAsO_4^{2-} ($\text{pK}_a = 6.97$) [31,45]. The electrostatic repulsion between oxyanions and the $\delta\text{-MnO}_2$ surface is the main cause for limited anion sorption. Manning et al. found that arsenate sorbed both on the edges and at the interlayer region of birnessite by forming bidentate binuclear corner-sharing complexes [60]. Several other studies proposed that arsenate only

sorbs on edge sites, and attributed the relatively low arsenate sorption to the limited amount of reactive edge sites for arsenate bonding [31,61]. Triple layer modeling results showed that the sorption of phosphate is unlikely to be inner-sphere, but rather through the formation of out-sphere complexation with MnO_x surface sites [45]. Wang et al. proposed that phosphate, silicate, and sulfate sorb on the edge sites of acid birnessite [62], but direct experimental confirmation (e.g., spectroscopic analysis) are still needed to confirm the actual binding mechanism(s) of phosphate on MnO_x [45].

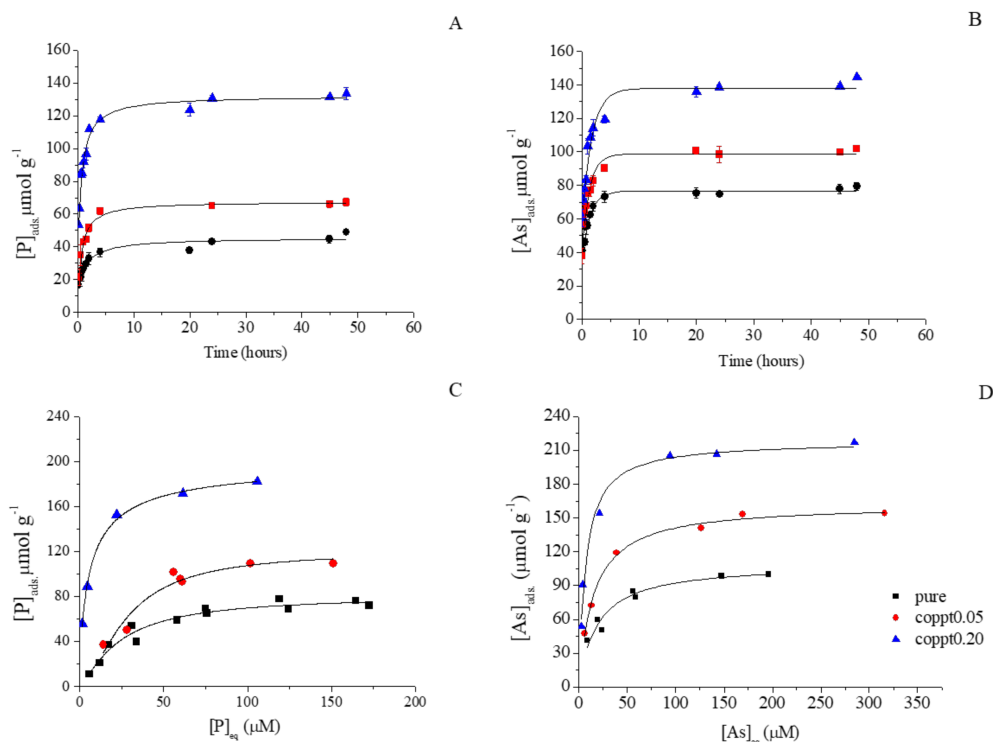


Figure 3. (A) Phosphate and (B) arsenate sorption kinetics on pure, coppt0.05, and coppt0.20 $\delta-MnO_2$ samples. Solid lines are pseudo first order model fitting results. (C) Phosphate and (D) arsenate sorption isotherms on pure, coppt0.05, and coppt0.20 $\delta-MnO_2$ samples. Initial phosphate and arsenate concentrations are 100 μM . Solid lines show the Langmuir fitting results. Error bars represent results from duplicates.

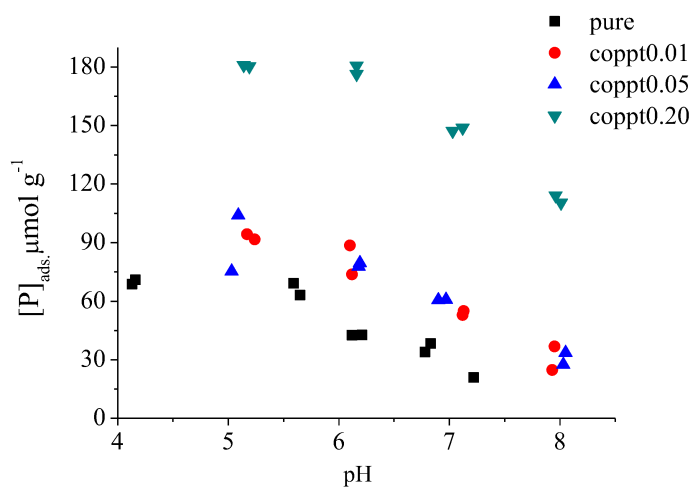


Figure 4. Phosphate sorption on pure, coppt0.05, and coppt0.20 $\delta-MnO_2$ samples as a function of pH. Initial phosphate concentration is 100 μM .

Table 3. Pseudo first order model fitting results for phosphate and arsenate sorption kinetics on pure and Zn co-precipitated δ -MnO₂.

Mn Oxide Type	P Kinetics			As Kinetics		
	k	Q _e	R ²	k	Q _e	R ²
pure	0.4217	43.4857	0.9176	0.6534	76.7312	0.9824
coppt0.05	0.6221	65.9621	0.9697	0.7433	98.7929	0.9495
coppt0.20	0.6936	128.688	0.9643	0.6985	137.8668	0.9615

3.2.2. Phosphate and Arsenate Sorption on Zn Coprecipitated δ -MnO₂

With increasing Zn concentration for Zn-coprecipitated δ -MnO₂, both phosphate and arsenate sorption were greatly enhanced (Figures 3 and 4). Based on the Langmuir model fitting results of sorption isotherms, the phosphate sorption capacity increased from 81.3 (pure δ -MnO₂) to 120.4 (coppt0.05) and 186.2 $\mu\text{mol g}^{-1}$ (coppt0.20). The arsenate sorption capacity increased from 109.4 (pure δ -MnO₂) to 162.2 (coppt0.05) and 218.0 $\mu\text{mol g}^{-1}$ (coppt0.20). The slopes of the sorption isotherms also became steeper with higher Zn treatment, suggesting that Zn-coprecipitation enhanced the affinity of anion sorbates. Such increased affinity was also manifested in the larger K values from Langmuir model fitting (Table 2). Enhanced phosphate and arsenate uptake by Zn-coprecipitated δ -MnO₂ was also observed for the kinetics and pH edge experiments. The sorption rate constants (k, Table 3) were higher for the coppt0.05 and coppt0.20 δ -MnO₂ samples, compared to that of pure δ -MnO₂. In Figure 4, the sorption edges of phosphate and arsenate shifted to higher pH values with increasing Zn content for Zn-coprecipitated δ -MnO₂. Previous studies showed that the phosphate sorption edges of hydrous MnO_x shifted to higher pH in Na⁺ and Ca²⁺ solutions or seawater, compared to that in water [45]. Co-existing metal cations [28] can also exert similar effects on phosphate sorption. Therefore, metal cations on MnO_x generally shift anion sorption edges to higher pH, regardless of cation species or whether the cation was added before or during anion sorption. This is possibly because cation sorption compensated for the negative surface charge of MnO_x, thus increasing anion affinity for the surface, or the potential formation of ternary complex (es) and/or precipitate(s).

In order to compare the influences of Zn-coprecipitation with Zn-sorption, Zn-sorbed δ -MnO₂ was prepared by mixing pure δ -MnO₂ with 0.25, 0.75, 1, and 2 mmol L⁻¹ Zn before anion sorption experiments. ICP-MS analysis of the supernatant suggested that 0.42, 0.99, 1.30, and 1.69 mmol g⁻¹ Zn was sorbed on δ -MnO₂, respectively (Table 1). δ -MnO₂ with increasing Zn loading showed enhanced phosphate and arsenate sorption capacities (Figure 5). Comparatively, the sorption capacity of Zn-coprecipitated coppt0.20 sample (with 1.5 mmol g⁻¹ Zn loading) for phosphate and arsenate was higher than that of all Zn-sorbed δ -MnO₂ samples, even though the Zn loading on the sorb0.60 sample was higher than that of the coppt0.20 sample (Figure 5). This confirms the significant influences of structural modifications caused by Zn-coprecipitation with δ -MnO₂.

3.3. Effect of Zn Coprecipitation on the Sorptive Reactivity of δ -MnO₂

3.3.1. Mechanisms for Cation Sorption on Zn-Coprecipitated δ -MnO₂

Previous studies have shown that sorbed Cd²⁺ on MnO_x existed as triple corner-sharing surface complexes below and/or above vacancy sites without incorporation into MnO_x layers [2,31,63]. Zn coprecipitation with δ -MnO₂ can affect Cd uptake by modifying surface charges, particle size, and vacancy site density. In previous studies, the effects of metal coprecipitation with birnessite on mineral sorptive reactivity are metal-specific, possibly depending on the ratio of metal incorporation/(surface complexation + incorporation), with Co 90–100%, Ni 10–45%, Cu 0–20%, and Zn 0% [2,27,63]. Co coprecipitation with MnO_x was shown to enhance Pb²⁺ sorption on birnessite [13] and cryptomelane [64], and the authors proposed that Co substitution of Mn(IV) led to a more negatively-charged surface and more sorption sites (hydroxyl groups in CoOOH). Compared to Co, Ni

coprecipitation with acid birnessite led to less Mn(IV) substitution (10–45% of Ni) vs. surface-sorbed species [27]. Surface-complexed Ni occupied surface vacancy sites and decreased the sorption capacity towards Zn^{2+} and Pb^{2+} [7]. Similar to the effects of coprecipitation, pre-sorbed metal cations can decrease MnO_x sorption capacity toward Pb^{2+} [26,65], Cu^{2+} , Zn^{2+} , and Cd^{2+} [26]. Zn was not observed to substitute or incorporate (0% of Zn) in δ - MnO_2 or phyllosmanganate layers, due to the large atomic difference between Zn and Mn(III, IV) and crystal field stabilization energy [2,27]. Therefore, Zn-coprecipitation could block surface vacancy sites, preventing further cation (e.g., Cd) sorption. Zn also compensated δ - MnO_2 negative surface charges (Figure S1 and Text S2), which also reduces the affinity between the cations (e.g., Cd) and the δ - MnO_2 surface.

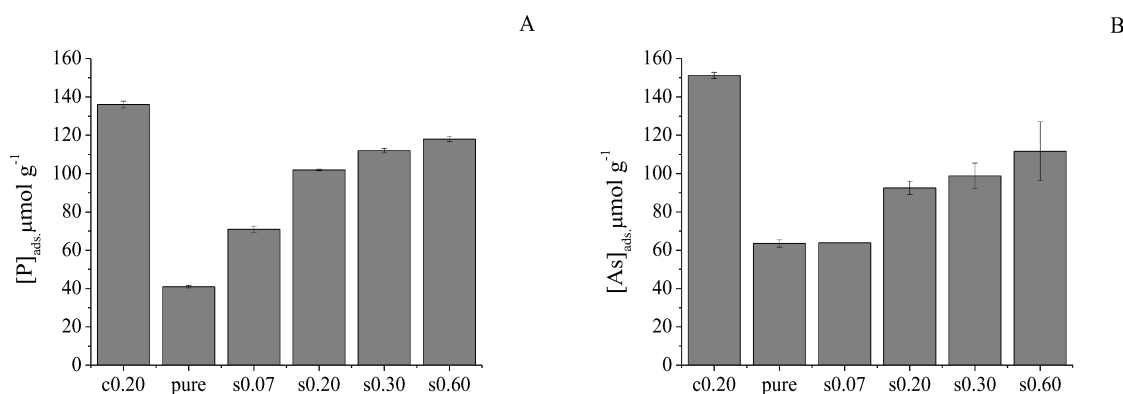


Figure 5. Comparison of phosphate and arsenate sorption on Zn-sorbed and 0.2Zn co-precipitated δ - MnO_2 (error bars represent results from duplicate experiments). “c” stands for “Zn-coprecipitation” samples and “s” for “Zn-sorption” samples. Initial phosphate and arsenate concentrations are 100 μM .

This study shows that Zn coprecipitated δ - MnO_2 possesses a larger sorptive capacity towards Cd than Zn-sorbed δ - MnO_2 at similar or even higher Zn loadings, suggesting that Zn coprecipitation not only blocked surface vacancy sites, but also affected the structural properties of δ - MnO_2 . Grangeon et al. found that Zn sorption can expel Mn(III) within δ - MnO_2 layers [21], leading to more vacancy sites and potentially increased sorption capacity towards metal cations [26]. Our recent study found that Zn coprecipitation had significant effects on δ - MnO_2 structure, causing a significantly reduced layer size and layer stacking and less Mn(III) occupation on vacancy sites [37]. These structural modifications might account for the higher total metal uptake by Zn-coprecipitated δ - MnO_2 than pure δ - MnO_2 . Yu et al. [36] also found more Zn uptake during biogenic MnO_x formation compared to Zn sorption on pre-formed biogenic MnO_x . It is likely that Zn inhibited the growth of fungal MnO_x and resulted in lower crystallinity MnO_x with a higher metal uptake capacity.

3.3.2. Solid Phase Analysis for Anion Sorption on Zn-Coprecipitated δ - MnO_2

XRD and As K-edge extended X-ray absorption fine edge structure (EXAFS) spectroscopy were conducted to characterize the solid products from sorption experiments, in order to explore the possible mechanisms underlying the effects of Zn-coprecipitation on sorptive reactivity. Pure δ - MnO_2 were mixed with 2 mmol L^{-1} Zn^{2+} (higher than coppt0.20 Zn loading) and 200 $\mu\text{mol L}^{-1}$ phosphate (highest phosphate concentration used in this study), and no bulk precipitation was identified by XRD (Figure S6). The rising peak at 1.6–1.9 \AA in the XRD spectra can be attributed to trace metal occupation on the vacancy sites [29].

Figure 6 shows the As EXAFS data of 100 $\mu\text{mol L}^{-1}$ arsenate sorption on 0.5 g L^{-1} pure and coppt0.20 δ - MnO_2 . No significant differences were observed for the spectra of the two samples. Fourier transformed (FT) spectra showed the two major peaks corresponding to As-O and As-Mn shells. Shell-by-shell fitting (Table S3) revealed ~ 4 oxygen atoms at ~ 1.69 \AA , consistent with the tetrahedral coordination of arsenate [31,60]. The second shell fitting indicated an As-Mn distance of 3.17–3.18 \AA ,

suggesting the formation of bidentate binuclear complex of As on δ -MnO₂ surfaces, consistent with the previously reported 3.17–3.22 Å range [31,60]. No additional pathways (e.g., As-Zn) were detected, suggesting no significant amount of ternary surface complex(es) and/or precipitation during arsenate sorption on Zn-coprecipitated δ -MnO₂. Previous EXAFS studies also did not find ternary complex formation among arsenate, MnO_x, and sorbed Zn/Pb [31], or precipitation of Mn²⁺ and arsenate produced during arsenite oxidation by MnO_x [66].

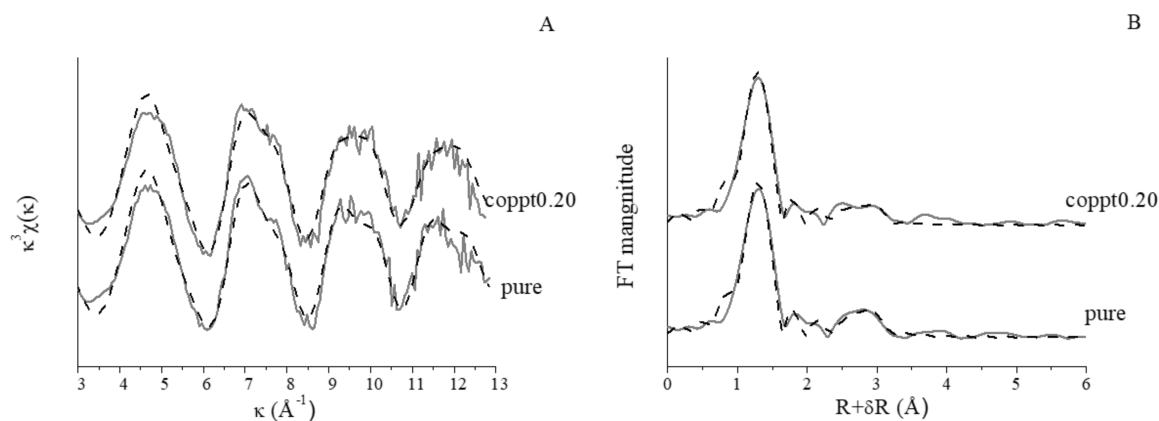


Figure 6. k^3 -weighted As extended X-ray absorption fine structure (EXAFS) spectroscopy (A) and Fourier transformed spectra (not corrected for phase shift) (B) of arsenate sorption on pure and coppt0.20 δ -MnO₂ samples. Raw and fitted data are in solid and dotted lines, respectively.

3.3.3. Mechanisms for Anion Sorption on Zn-Coprecipitated δ -MnO₂

Metal cations can influence phosphate and arsenate sorption in several ways. First, pre-existing cations on the δ -MnO₂ surface might compete with anions for sorption sites. Yao et al. proposed that Ca²⁺ and Mg²⁺ can suppress phosphate sorption on hydrous MnO_x by occupying surface sites and forming phosphate complexes in the solution [45]. Power et al. found that sorbed Zn²⁺ slowed down arsenite oxidation by blocking δ -MnO₂ surface sites for arsenite complexation and electron transfer [30]. To verify the presence of competitive sorption, we monitored the release of metals (Zn and total Mn) from the coppt0.20 sample equilibrated with 10 mmol L⁻¹ NaCl solution with or without 100 μ mol L⁻¹ phosphate (Figure S7). Mn was not detected in the solution. Desorbed Zn was \sim 9 μ mol L⁻¹ when 0.2coppt birnessite was equilibrated with 100 μ mol L⁻¹ phosphate and \sim 8 μ mol L⁻¹ without P after 24 h (Figure S7). Phosphate did not induce substantial Zn desorption, suggesting little competition between Zn and phosphate, likely due to the different sorption sites that they prefer. Zn sorbs mostly at interlayer vacancy sites [21,67], while anions such as phosphate, silicate, and sulfate are generally considered to complex at edge sites of birnessite layers [62].

Secondly, the presence of metal cations may compensate the negative surface charge of δ -MnO₂, thus reducing the electrostatic repulsion between δ -MnO₂ surface and anions and enhancing anion sorption. In general, anion uptake by negatively-charged Mn oxides is limited, and anions are more likely to be associated with more positively charged Fe and Al (oxyhydr)oxides [68–70]. However, charge compensation through cation sorption/coprecipitation can significantly enhance anion sorption on MnO_x. Vilallobos et al. found that Zn²⁺ and Pb²⁺ sorption on δ -MnO₂ and birnessite enhanced the sorption of arsenate [31]. Kawashima et al. [28] found that co-existing Ca²⁺, Mg²⁺, Ba²⁺, Sr²⁺, Mn²⁺, Co²⁺, and Ni²⁺ greatly enhanced phosphate sorption on hydrous MnO_x over a wide range of pH. The order of enhancement by alkaline earth elements is Ba²⁺ > Sr²⁺ > Ca²⁺ > Mg²⁺, suggesting that cations with smaller hydrated radii (i.e., higher charge density) are more likely to promote anion sorption. A previous study showed that in seawater (containing concentrated Ca²⁺, Na⁺, K⁺, Mg²⁺, and other metal cations), phosphate uptake by hydrous Mn oxides was comparable to that by goethite, and even higher than goethite at pH < 4 [45]. Mn²⁺-rich hydrous Mn oxides were also shown to play

important roles in As accumulation in Biwa lake sediments in Japan [71]. The study suggested that, since Mn oxides are important oxidants for arsenite, the resulting arsenate can accumulate on MnO_x surfaces that are charge compensated by cations (Mn, Ni, and earth alkaline cations).

Thirdly, the common presence of metals during MnO_x formation in the natural environment is likely to modify the MnO_x structure and enhance the anion uptake capacity, especially metals with limited incorporation into MnO_x vacancy sites such as Zn and Ni [11]. As discussed above, Zn-sorption was not as effective as Zn-coprecipitation for the enhancement of phosphate and arsenate sorption on $\delta\text{-MnO}_2$, due to the structural modifications by Zn-coprecipitation. Zn sorption was shown to cause $\delta\text{-MnO}_2$ dissolution and caused 15–20% reduction in the lateral coherent domain size after ~12 h at pH 5–7 [21]. Zn coprecipitation caused even greater effects on the $\delta\text{-MnO}_2$ layer structure [37]. Reduced layer size can expose more available edges for anions, which mostly sorb onto edge sites [31].

4. Conclusions

In this study, Cd was chosen as a cation probe while phosphate and arsenate were chosen as anion probes to investigate the effects of Zn-coprecipitation on the sorptive reactivity of $\delta\text{-MnO}_2$. Compared to pure $\delta\text{-MnO}_2$, Zn-coprecipitated $\delta\text{-MnO}_2$ phases are less negatively charged, and have a smaller layer size and less layer Mn(III) occupation on vacancy sites. Pre-loaded Zn, either coprecipitated or sorbed, inhibited Cd sorption on $\delta\text{-MnO}_2$, due to the competition between Zn and Cd. Total metal uptake (Zn + Cd) was enhanced as a result of the above-mentioned structural changes. Zn-sorbed $\delta\text{-MnO}_2$ has a smaller Cd sorption capacity than Zn-coprecipitated $\delta\text{-MnO}_2$, even if the latter has less pre-loaded Zn. The charge-compensated Zn- $\delta\text{-MnO}_2$ surface showed significantly enhanced sorptive capacity toward the anions phosphate and arsenate. Higher sorption capacity, higher affinity, faster kinetics, and a right-shifted sorption edge were observed for phosphate and arsenate sorption on Zn-coprecipitated $\delta\text{-MnO}_2$, compared to pure $\delta\text{-MnO}_2$. Compared to Zn-sorbed $\delta\text{-MnO}_2$ samples, Zn-coprecipitation was more effective in enhancing anion sorption. No significant amount of ternary surface complex and/or precipitates were detected for phosphate and arsenate sorption on Zn treated $\delta\text{-MnO}_2$. This study quantified the sorptive reactivities of MnO_x under complex conditions close to realistic environments and revealed the underlying mechanisms. Our study suggests that the roles of MnO_x in regulating anion fate and transport should be re-visited by considering the impacts (e.g., structural modification, surface charge compensation) of metal presence during (i.e., coprecipitation) and after MnO_x formation (i.e., sorption). As metal coprecipitation with MnO_x minerals can be a common environmental process, our findings can help better understand the roles of MnO_x in the biogeochemical cycles of nutrients, metals and organic contaminants.

Supplementary Materials: The following are available online at <http://www.mdpi.com/2411-5126/2/2/19/s1>. XRD and XAS experiment details; summary of $\delta\text{-MnO}_2$ structure modifications by Zn coprecipitation (e.g., surface charge measurements); Zn and Cd sorption on pure $\delta\text{-MnO}_2$; Sorption isotherm normalized by BET surface area instead of by mass; fitting results of cation and anion sorption isotherms and kinetics using different sorption models; shell-by-shell fitting results of As EXAFS spectra; Zn release from Zn-coprecipitated $\delta\text{-MnO}_2$ with and without the presence of phosphate.

Acknowledgments: We acknowledge funding support from NASA grant #NNA15BB03A and NSF grant #1710285. We appreciate the support from beamline scientist Qing Ma at APS Beamline 5-BM-D. Portions of this research were conducted at the Advanced Photon Source (APS). Use of the Advanced Photon Source was supported by the U.S. Department of Energy, Office of Science and Office of Basic Energy Sciences.

Author Contributions: Yuanzhi Tang and Shiliang Zhao conceived and designed the experiments; Shiliang Zhao and Chenning Li performed the experiments and analyzed the data; Pan Liu, Rixiang Huang, and Emily Saad contributed to sample analysis; Shiliang Zhao wrote the paper; Yuanzhi Tang and Rixiang Huang edited the paper.

Conflicts of Interest: The authors declare no conflict of interest.

References

1. Taylor, R.; McKenzie, R.; Norrish, K. The mineralogy and chemistry of manganese in some Australian soils. *Soil Res.* **1964**, *2*, 235–248. [CrossRef]

2. Manceau, A.; Lanson, B.; Drits, V.A. Structure of heavy metal sorbed birnessite. Part III: Results from powder and polarized extended X-ray absorption fine structure spectroscopy. *Geochim. Cosmochim. Acta* **2002**, *66*, 2639–2663. [[CrossRef](#)]
3. Huang, P. Kinetics of redox reactions on manganese oxides and its impact on environmental quality. In *Rates of Soil Chemical Processes*; Soil Science Society of America: Madison, WI, USA, 1991; pp. 191–230.
4. Trivedi, P.; Axe, L.; Tyson, T.A. XAS Studies of Ni and Zn Sorbed to Hydrous Manganese Oxide. *Environ. Sci. Technol.* **2001**, *35*, 4515–4521. [[CrossRef](#)] [[PubMed](#)]
5. Peacock, C.L.; Sherman, D.M. Sorption of Ni by birnessite: Equilibrium controls on Ni in seawater. *Chem. Geol.* **2007**, *238*, 94–106. [[CrossRef](#)]
6. Jenne, E.A. Controls on Mn, Fe, Co, Ni, Cu, and Zn concentrations in soils and water: The significant role of hydrous Mn and Fe oxides. *Adv. Chem.* **1968**, *73*, 337–387.
7. Yin, H.; Tan, W.; Zheng, L.; Cui, H.; Qiu, G.; Liu, F.; Feng, X. Characterization of Ni-rich hexagonal birnessite and its geochemical effects on aqueous Pb^{2+}/Zn^{2+} and As (III). *Geochim. Cosmochim. Acta* **2012**, *93*, 47–62. [[CrossRef](#)]
8. Decrée, S.; Pourret, O.; Baele, J.-M. Rare earth element fractionation in heterogenite (CoOOH): Implication for cobalt oxidized ore in the Katanga Copperbelt (Democratic Republic of Congo). *J. Geochem. Explor.* **2015**, *159*, 290–301. [[CrossRef](#)]
9. Manceau, A.; Silvester, E.; Bartoli, C.; Lanson, B.; Drits, V.A. Structural mechanism of Co^{2+} oxidation by the phyllo-manganate buserite. *Am. Mineral.* **1997**, *82*, 1150–1175. [[CrossRef](#)]
10. Yin, H.; Liu, Y.; Koopal, L.K.; Feng, X.; Chu, S.; Zhu, M.; Liu, F. High Co-doping promotes the transition of birnessite layer symmetry from orthogonal to hexagonal. *Chem. Geol.* **2015**, *410*, 12–20. [[CrossRef](#)]
11. Yin, H.; Liu, F.; Feng, X.; Hu, T.; Zheng, L.; Qiu, G.; Koopal, L.K.; Tan, W. Effects of Fe doping on the structures and properties of hexagonal birnessites—Comparison with Co and Ni doping. *Geochim. Cosmochim. Acta* **2013**, *117*, 1–15. [[CrossRef](#)]
12. Manceau, A.; Llorca, S.; Calas, G. Crystal chemistry of cobalt and nickel in lithiophorite and asbolane from New Caledonia. *Geochim. Cosmochim. Acta* **1987**, *51*, 105–113. [[CrossRef](#)]
13. Yin, H.; Feng, X.; Qiu, G.; Tan, W.; Liu, F. Characterization of Co-doped birnessites and application for removal of lead and arsenite. *J. Hazard. Mater.* **2011**, *188*, 341–349. [[CrossRef](#)] [[PubMed](#)]
14. Kwon, K.D.; Refson, K.; Sposito, G. Surface complexation of Pb (II) by hexagonal birnessite nanoparticles. *Geochim. Cosmochim. Acta* **2010**, *74*, 6731–6740. [[CrossRef](#)]
15. Yin, H.; Feng, X.; Tan, W.; Koopal, L.K.; Hu, T.; Zhu, M.; Liu, F. Structure and properties of vanadium (V)-doped hexagonal turbostratic birnessite and its enhanced scavenging of Pb^{2+} from solutions. *J. Hazard. Mater.* **2015**, *288*, 80–88. [[CrossRef](#)] [[PubMed](#)]
16. Nelson, Y.M.; Lion, L.W.; Ghiorse, W.C.; Shuler, M.L. Production of biogenic Mn oxides by *Leptothrix discophora* SS-1 in a chemically defined growth medium and evaluation of their Pb adsorption characteristics. *Appl. Environ. Microbiol.* **1999**, *65*, 175–180. [[PubMed](#)]
17. Zhao, W.; Wang, Q.Q.; Liu, F.; Qiu, G.H.; Tan, W.F.; Feng, X.H. Pb^{2+} adsorption on birnessite affected by Zn^{2+} and Mn^{2+} pretreatments. *J. Soils Sediments* **2010**, *10*, 870–878. [[CrossRef](#)]
18. Villalobos, M.; Bargar, J.; Sposito, G. Mechanisms of Pb (II) sorption on a biogenic manganese oxide. *Environ. Sci. Technol.* **2005**, *39*, 569–576. [[CrossRef](#)] [[PubMed](#)]
19. Peña, J.; Bargar, J.R.; Sposito, G. Copper sorption by the edge surfaces of synthetic birnessite nanoparticles. *Chem. Geol.* **2015**, *396*, 196–207. [[CrossRef](#)]
20. Sherman, D.M.; Peacock, C.L. Surface complexation of Cu on birnessite (δ - MnO_2): Controls on Cu in the deep ocean. *Geochim. Cosmochim. Acta* **2010**, *74*, 6721–6730. [[CrossRef](#)]
21. Grangeon, S.; Manceau, A.; Guilhermet, J.; Gaillot, A.-C.; Lanson, M.; Lanson, B. Zn sorption modifies dynamically the layer and interlayer structure of vernadite. *Geochim. Cosmochim. Acta* **2012**, *85*, 302–313. [[CrossRef](#)]
22. Boonfueng, T.; Axe, L.; Yee, N.; Hahn, D.; Ndiba, P.K. Zn sorption mechanisms onto sheathed *Leptothrix discophora* and the impact of the nanoparticulate biogenic Mn oxide coating. *J. Colloid Interface Sci.* **2009**, *333*, 439–447. [[CrossRef](#)] [[PubMed](#)]
23. Chang, J.; Tani, Y.; Naitou, H.; Miyata, N.; Tojo, F.; Seyama, H. Zn (II) sequestration by fungal biogenic manganese oxide through enzymatic and abiotic processes. *Chem. Geol.* **2014**, *383*, 155–163. [[CrossRef](#)]
24. Trivedi, P.; Axe, L. Modeling Cd and Zn sorption to hydrous metal oxides. *Environ. Sci. Technol.* **2000**, *34*, 2215–2223. [[CrossRef](#)]

25. Tripathy, S.S.; Bersillon, J.-L.; Gopal, K. Adsorption of Cd^{2+} on hydrous manganese dioxide from aqueous solutions. *Desalination* **2006**, *194*, 11–21. [[CrossRef](#)]
26. Wang, Y.; Feng, X.; Villalobos, M.; Tan, W.; Liu, F. Sorption behavior of heavy metals on birnessite: Relationship with its Mn average oxidation state and implications for types of sorption sites. *Chem. Geol.* **2012**, *292–293*, 25–34. [[CrossRef](#)]
27. Kwon, K.D.; Refson, K.; Sposito, G. Understanding the trends in transition metal sorption by vacancy sites in birnessite. *Geochim. Cosmochim. Acta* **2013**, *101*, 222–232. [[CrossRef](#)]
28. Kawashima, M.; Tainaka, Y.; Hori, T.; Koyama, M.; Takamatsu, T. Phosphate adsorption onto hydrous manganese(IV) oxide in the presence of divalent cations. *Water Res.* **1986**, *20*, 471–475. [[CrossRef](#)]
29. Grangeon, S.; Lanson, B.; Lanson, M.; Manceau, A. Crystal structure of Ni-sorbed synthetic vernadite: A powder X-ray diffraction study. *Mineral. Mag.* **2008**, *72*, 1279–1291. [[CrossRef](#)]
30. Power, L.E.; Arai, Y.; Sparks, D.L. Zinc adsorption effects on arsenite oxidation kinetics at the birnessite-water interface. *Environ. Sci. Technol.* **2005**, *39*, 181–187. [[CrossRef](#)] [[PubMed](#)]
31. Villalobos, M.; Escobar-Quiroz, I.N.; Salazar-Camacho, C. The influence of particle size and structure on the sorption and oxidation behavior of birnessite: I. Adsorption of As (V) and oxidation of As (III). *Geochim. Cosmochim. Acta* **2014**, *125*, 564–581. [[CrossRef](#)]
32. Qin, Z.; Xiang, Q.; Liu, F.; Xiong, J.; Koopal, L.K.; Zheng, L.; Ginder-Vogel, M.; Wang, M.; Feng, X.; Tan, W. Local structure of Cu^{2+} in Cu-doped hexagonal turbostratic birnessite and Cu^{2+} stability under acid treatment. *Chem. Geol.* **2017**, *466*, 512–523. [[CrossRef](#)]
33. Opfergelt, S.; Cornéilis, J.-T.; Houben, D.; Givron, C.; Burton, K.; Mattielli, N. The influence of weathering and soil organic matter on Zn isotopes in soils. *Chem. Geol.* **2017**, *466*, 140–148. [[CrossRef](#)]
34. Hinkle, M.A.; Dye, K.G.; Catalano, J.G. Impact of Mn (II)-Manganese Oxide Reactions on Ni and Zn Speciation. *Environ. Sci. Technol.* **2017**, *51*, 3187–3196. [[CrossRef](#)] [[PubMed](#)]
35. Drits, V.A.; Lanson, B.; Bougerol-Chaillout, C.; Gorshkov, A.I.; Manceau, A. Structure of heavy-metal sorbed birnessite: Part 2. Results from electron diffraction. *Am. Mineral.* **2002**, *87*, 1646–1661. [[CrossRef](#)]
36. Yu, Q.; Sasaki, K.; Tanaka, K.; Ohnuki, T.; Hirajima, T. Zinc sorption during bio-oxidation and precipitation of manganese modifies the layer stacking of biogenic birnessite. *Geomicrobiol. J.* **2013**, *30*, 829–839. [[CrossRef](#)]
37. Zhao, S.; Wang, Q.; Sun, J.; Borkiewicz, O.; Huang, R.; Saad, E.; Fields, B.; Chen, S.; Zhu, M.; Tang, Y. Effect of Zn^{2+} presence during mineral formation on the structure of layered Mn oxides. *Chem. Geol.* Submitted in 2017.
38. Jenkyns, H.C. Fossil manganese nodules from the west Sicilian Jurassic. *Ecoloe Geol. Helv.* **1970**, *63*, 741–774.
39. Childs, C.W. Composition of iron-manganese concretions from some New Zealand soils. *Geoderma* **1975**, *13*, 141–152. [[CrossRef](#)]
40. Manceau, A.; Tamura, N.; Celestre, R.S.; MacDowell, A.A.; Geoffroy, N.; Sposito, G.; Padmore, H.A. Molecular-scale speciation of Zn and Ni in soil ferromanganese nodules from loess soils of the Mississippi Basin. *Environ. Sci. Technol.* **2003**, *37*, 75–80. [[CrossRef](#)] [[PubMed](#)]
41. Tan, H.; Zhang, G.; Heaney, P.J.; Webb, S.M.; Burgos, W.D. Characterization of manganese oxide precipitates from Appalachian coal mine drainage treatment systems. *Appl. Geochem.* **2010**, *25*, 389–399. [[CrossRef](#)]
42. Lanson, B.; Marcus, M.A.; Fakra, S.; Panfili, F.; Geoffroy, N.; Manceau, A. Formation of Zn–Ca phyllomanganate nanoparticles in grass roots. *Geochim. Cosmochim. Acta* **2008**, *72*, 2478–2490. [[CrossRef](#)]
43. Meng, Y.-T.; Zheng, Y.-M.; Zhang, L.-M.; He, J.-Z. Biogenic Mn oxides for effective adsorption of Cd from aquatic environment. *Environ. Pollut.* **2009**, *157*, 2577–2583. [[CrossRef](#)] [[PubMed](#)]
44. Dong, D.; Li, Y.; Hua, X. Investigation of Fe, Mn oxides and organic material in surface coatings and Pb, Cd adsorption to surface coatings developed in different natural waters. *Microchem. J.* **2001**, *70*, 25–33. [[CrossRef](#)]
45. Yao, W.; Millero, F.J. Adsorption of Phosphate on Manganese Dioxide in Seawater. *Environ. Sci. Technol.* **1996**, *30*, 536–541. [[CrossRef](#)]
46. Violante, A.; Pigna, M. Competitive sorption of arsenate and phosphate on different clay minerals and soils. *Soil Sci. Soc. Am. J.* **2002**, *66*, 1788–1796. [[CrossRef](#)]
47. Liu, F.; De Cristofaro, A.; Violante, A. Effect of pH, phosphate and oxalate on the adsorption/desorption of arsenate on/from goethite. *Soil Sci.* **2001**, *166*, 197–208. [[CrossRef](#)]
48. Baldwin, D.S.; Beattie, J.K.; Coleman, L.M.; Jones, D.R. Hydrolysis of an organophosphate ester by manganese dioxide. *Environ. Sci. Technol.* **2001**, *35*, 713–716. [[CrossRef](#)] [[PubMed](#)]

49. McCarty, K.M.; Hanh, H.T.; Kim, K.W. Arsenic geochemistry and human health in South East Asia. *Rev. Environ. Health* **2011**, *26*, 71–78. [[CrossRef](#)] [[PubMed](#)]
50. Watanabe, J.I.; Tani, Y.; Miyata, N.; Seyama, H.; Mitsunobu, S.; Naitou, H. Concurrent sorption of As (V) and Mn (II) during biogenic manganese oxide formation. *Chem. Geol.* **2012**, *306*, 123–128. [[CrossRef](#)]
51. Marcus, M.A.; Manceau, A.; Kersten, M. Mn, Fe, Zn and As speciation in a fast-growing ferromanganese marine nodule. *Geochim. Cosmochim. Acta* **2004**, *68*, 3125–3136. [[CrossRef](#)]
52. Zhu, M.; Farrow, C.L.; Post, J.E.; Livi, K.J.T.; Billinge, S.J.L.; Ginder-Vogel, M.; Sparks, D.L. Structural study of biotic and abiotic poorly-crystalline manganese oxides using atomic pair distribution function analysis. *Geochim. Cosmochim. Acta* **2012**, *81*, 39–55. [[CrossRef](#)]
53. Murphy, J.; Riley, J. A modified single solution method for determination of phosphate uptake by rye. *Soil Sci. Soc. Am. Proc.* **1952**, *48*, 31–36.
54. Lenoble, V.; Deluchat, V.; Serpaud, B.; Bollinger, J.-C. Arsenite oxidation and arsenate determination by the molybdene blue method. *Talanta* **2003**, *61*, 267–276. [[CrossRef](#)]
55. Balistrieri, L.S.; Chao, T. Adsorption of selenium by amorphous iron oxyhydroxide and manganese dioxide. *Geochim. Cosmochim. Acta* **1990**, *54*, 739–751. [[CrossRef](#)]
56. Mustafa, S.; Zaman, M.I.; Khan, S. pH effect on phosphate sorption by crystalline MnO₂. *J. Colloid Interface Sci.* **2006**, *301*, 370–375. [[CrossRef](#)] [[PubMed](#)]
57. Mustafa, S.; Zaman, M.I.; Khan, S. Temperature effect on the mechanism of phosphate anions sorption by β -MnO₂. *Chem. Eng. J.* **2008**, *141*, 51–57. [[CrossRef](#)]
58. Ouvrard, S.; Simonnot, M.-O.; Sardin, M. Reactive behavior of natural manganese oxides toward the adsorption of phosphate and arsenate. *Ind. Eng. Chem. Res.* **2002**, *41*, 2785–2791. [[CrossRef](#)]
59. Sparks, D.L. *Environmental Soil Chemistry*; Academic Press: Cambridge, MA, USA, 2002.
60. Manning, B.A.; Fendorf, S.E.; Bostick, B.; Suarez, D.L. Arsenic (III) oxidation and arsenic (V) adsorption reactions on synthetic birnessite. *Environ. Sci. Technol.* **2002**, *36*, 976–981. [[CrossRef](#)] [[PubMed](#)]
61. Deschamps, E.; Ciminelli, V.S.; Weidler, P.G.; Ramos, A.Y. Arsenic sorption onto soils enriched in Mn and Fe minerals. *Clays Clay Miner.* **2003**, *51*, 197–204. [[CrossRef](#)]
62. Wang, Q.; Liao, X.; Xu, W.; Ren, Y.; Livi, K.J.; Zhu, M. Synthesis of Birnessite in the Presence of Phosphate, Silicate, or Sulfate. *Inorg. Chem.* **2016**, *55*, 10248–10258. [[CrossRef](#)] [[PubMed](#)]
63. Lanson, B.; Drits, V.A.; Gaillot, A.-C.; Silvester, E.; Plançon, A.; Manceau, A. Structure of heavy-metal sorbed birnessite: Part 1. Results from X-ray diffraction. *Am. Mineral.* **2002**, *87*, 1631–1645. [[CrossRef](#)]
64. Li, H.; Liu, F.; Zhu, M.; Feng, X.; Zhang, J.; Yin, H. Structure and properties of Co-doped cryptomelane and its enhanced removal of Pb²⁺ and Cr³⁺ from wastewater. *J. Environ. Sci.* **2015**, *34*, 77–85. [[CrossRef](#)] [[PubMed](#)]
65. Yin, H.; Liu, F.; Feng, X.; Liu, M.; Tan, W.; Qiu, G. Co²⁺-exchange mechanism of birnessite and its application for the removal of Pb²⁺ and As (III). *J. Hazard. Mater.* **2011**, *196*, 318–326. [[CrossRef](#)] [[PubMed](#)]
66. Lafferty, B.J.; Ginder-Vogel, M.; Zhu, M.; Livi, K.J.; Sparks, D.L. Arsenite oxidation by a poorly crystalline manganese-oxide. 2. Results from X-ray absorption spectroscopy and X-ray diffraction. *Environ. Sci. Technol.* **2010**, *44*, 8467–8472. [[CrossRef](#)] [[PubMed](#)]
67. Kwon, K.D.; Refson, K.; Sposito, G. Zinc surface complexes on birnessite: A density functional theory study. *Geochim. Cosmochim. Acta* **2009**, *73*, 1273–1284. [[CrossRef](#)]
68. Zeng, L.; Li, X.; Liu, J. Adsorptive removal of phosphate from aqueous solutions using iron oxide tailings. *Water Res.* **2004**, *38*, 1318–1326. [[CrossRef](#)] [[PubMed](#)]
69. Tanada, S.; Kabayama, M.; Kawasaki, N.; Sakiyama, T.; Nakamura, T.; Araki, M.; Tamura, T. Removal of phosphate by aluminum oxide hydroxide. *J. Colloid Interface Sci.* **2003**, *257*, 135–140. [[CrossRef](#)]
70. Dixit, S.; Hering, J.G. Comparison of arsenic (V) and arsenic (III) sorption onto iron oxide minerals: Implications for arsenic mobility. *Environ. Sci. Technol.* **2003**, *37*, 4182–4189. [[CrossRef](#)] [[PubMed](#)]
71. Takamatsu, T.; Kawashima, M.; Koyama, M. The role of Mn²⁺-rich hydrous manganese oxide in the accumulation of arsenic in lake sediments. *Water Res.* **1985**, *19*, 1029–1032. [[CrossRef](#)]

